Bioorganic Chemistry 89 (2019) 103019

Contents lists available at ScienceDirect

Bioorganic Chemistry

journal homepage: www.elsevier.com/locate/bioorg

A bright blue fluorescent dextran for two-photon *in vivo* imaging of blood vessels

Seo Hyeon Lee[a,1], Young Ho Choe[b,1], Rae Hyung Kang[a,1], Yu Rim Kim[b], Na Hee Kim[a], Sangrim Kang[c], Youngseo Kim[d], Sungnam Park[d], Young-Min Hyun[b,*], Dokyoung Kim[a,c,e,f,*]

[a] Department of Biomedical Science, Graduate School, Kyung Hee University, Seoul 02447, Republic of Korea
[b] Department of Anatomy and Brain Korea 21 PLUS Project for Medicine Science, Yonsei University, College of Medicine, Seoul 03722, Republic of Korea
[c] Department of Anatomy and Neurobiology, College of Medicine, Kyung Hee University, Seoul 02447, Republic of Korea
[d] Department of Chemistry, Korea University, Seoul 02841, Republic of Korea
[e] Center for Converging Humanities, Kyung Hee University, Seoul 02447, Republic of Korea
[f] Medical Research Center for Bioreaction to Reactive Oxygen Species and Biomedical Science Institute, Kyung Hee University, Seoul 02447, Republic of Korea

ARTICLE INFO

Keywords:
Blood vessel staining
Blue-emitting dextran
Two-photon imaging
Fluorescent polymer
In vivo imaging

ABSTRACT

Fluorescence-based *in vivo* imaging is one of the most important tools for monitoring of biological processes in cells and tissues of live animal models. Fluorescence imaging agents have also been used to monitor the microcirculation. Tracking microcirculation of the blood is vital to gain further insight into various vascular disease-related anomalies within the human body. As monitoring of vascular circulation is performed with visualization of both immune cells and pathogens, which are mainly labelled with red and green, the favorable color option for blood vessels could be blue. However, currently available blueish color-labeled agents for vascular monitoring is generally confronted with quick bleaching, because of its short excitation and emission wavelengths. Hereby, what we propose in this report is a newly generated bright blue fluorescent dextran, named HCD-70K that monitors the blood vessels using blue and inter-compatible typical fluorescent materials. DBCO-functionalized dextran-70K was fabricated with hydroxy-coumarin dye via metal-free bioorthogonal click chemistry, and generated HCD-70K, which can flow within the blood vessel and decipher the whole structure of the blood vessel successfully. The synthesis, spectroscopic analysis, and quantum chemical calculations were conducted. Using two-photon microscopy, efficient deep *in vivo* blood vessel imaging of a mouse model revealed exceptional bio-imaging capabilities of the HCD-70K and consequently it provided a promising opportunity for efficient vascular visualization in various research areas.

1. Introduction

Tracking microcirculation of the blood is crucial for understanding various vascular disease-related phenomena in the body. Many cardiovascular, pulmonary vascular and renal diseases are manifested by immune reactions due to abnormal blood flow [1–4]. To highlight the intact blood stream in the blood vessel, many imaging techniques and agents have been reported in the field of magnetic resonance imaging (MRI) [5], computed tomography (CT) [6], positron emission tomography (PET) [7], photoacoustic imaging (PAI) [8], and two-photon microscopy (TPM) *in vivo* imaging [9].

The most widely used *in vivo* imaging in basic research is TPM, due to its excellent performances within the animal model such as the high resolution 3-D imaging, fast-response, deep tissue imaging, less photo-damage and photo-bleaching, as well as being highly adaptable to biological species [10–14]. In previous studies, a formulation, such as organic fluorophore (i.e. FITC, TRITC, cyanine, Texas red) conjugated bio-applicable polymer (i.e. dextran) [15] and fluorophore-protein agglomerate (i.e. Evans blue with albumin) [9,16–20] were used to visualize the blood flow (Fig. S1 in Supplementary Information; SI). In addition, antibody with affinity to typical endothelial marker CD31 (PECAM-1) or lectin wheat germ agglutinin (WGA) with selective affinity to *N*-acetyl-D-glucosamine and sialic acid were used to visualize the blood vessel [21–23]. However, in order to stain the whole blood vessel, large amounts of antibody needs to be injected intravenously to circulate throughout the body. Moreover, the lectin binds not only to the wall of blood vessels but also to other cells. Another limitation for these fluorescent materials is that the commercially available

* Corresponding authors at: Department of Biomedical Science, Graduate School, Kyung Hee University, Seoul 02447, Republic of Korea (D. Kim).
E-mail addresses: ymhyun@yuhs.ac (Y.-M. Hyun), dkim@khu.ac.kr (D. Kim).
[1] These authors contributed equally.

https://doi.org/10.1016/j.bioorg.2019.103019
Received 13 March 2019; Received in revised form 1 May 2019; Accepted 28 May 2019
Available online 30 May 2019
0045-2068/

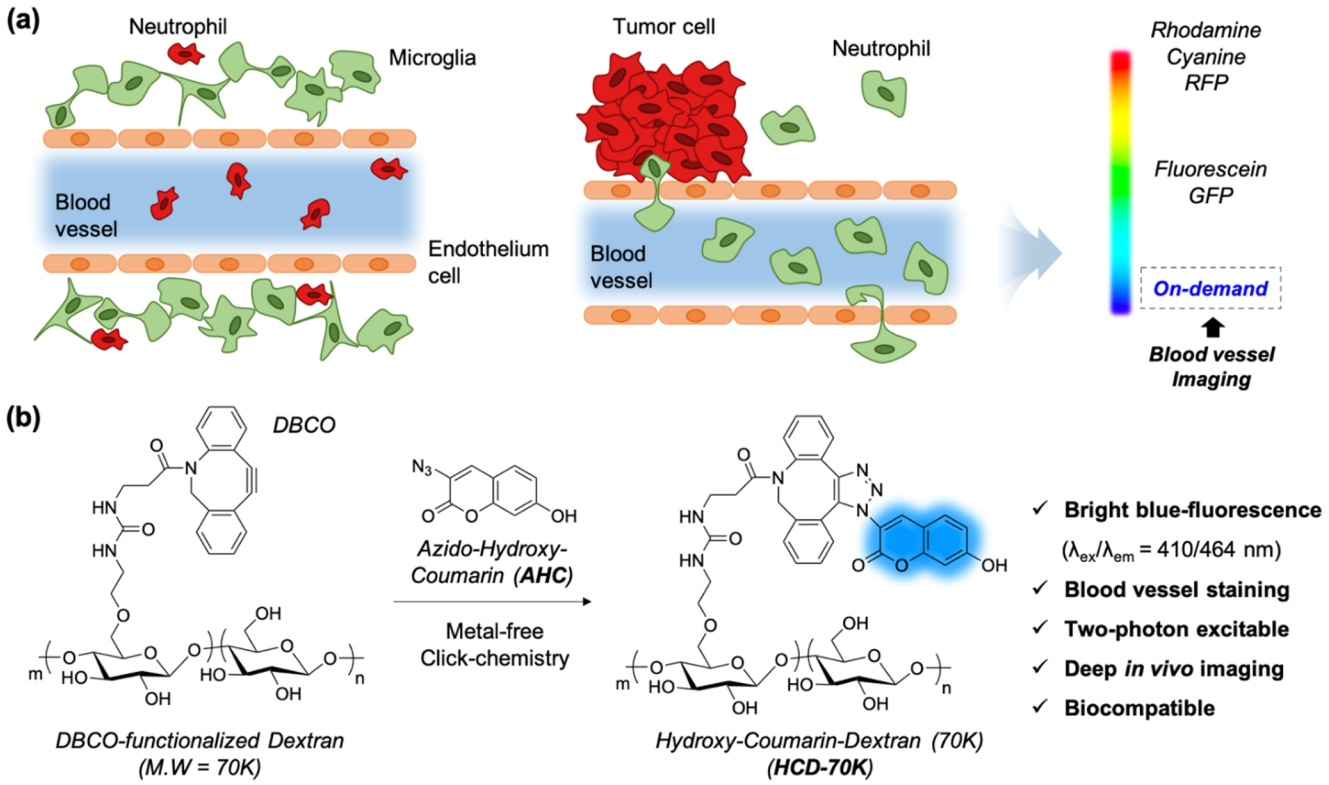

Fig. 1. (a) Schematic illustration for fluorescence imaging of neutrophil, microglia, tumor cell, and blood vessel. (b) Structure and synthetic method for blue-emitting dextran (M.W = 70 kDa, **HCD-70K**). The key features are summarized.

fluorescent blood vessel imaging agents mainly have green- or red-emitting properties, which are commonly used for the staining of immune cells from GFP-expressing neutrophil or macrophage bearing mice or red-fluorescent protein expressing cancer cells through genetic modification (Fig. 1a). Therefore, these overlapping fluorescence emissions reduce the opportunity to label the blood vessel with these green- or red-fluorescent reagents. This is because the cells circulating in the blood vessels already have one of these fluorescent tags. Due to this reason, it is on high demand to develop blue-emitting, two-photon absorbing, deep and stable *in vivo* imaging, under physiological conditions, and blood vessel selective imaging agents.

In this study, we report a newly designed bright blue fluorescent dextran formulation in order to overcome the issues described above in detail. Dextran-70K (M.W = 70 kDa) is similar to bovine serum albumin (BSA) in its molecular weight and can be used in various research fields because it can be carried through the blood stream for a long time without escaping from the vessels [16–18]. The blue fluorescence is derived from the hydroxy-coumarin moiety that conjugated to the dextran backbone (Fig. 1b). The prepared formulation, named **HCD-70K**, shows an absorption and fluorescence emission throughout the blue wavelength range ($\lambda_{abs.max}$ = 404 nm, $\lambda_{emi.max}$ = 464 nm). With this noble coumarin conjugated dextran, we have proved that it was less cytotoxic and did not interfere with other green- or red-emitting fluorophores, and had stable fluorescence intensity when injected into the blood vessel. Using two-photon *in vivo* microscopy, we were able to successfully see the correlation between the blood flow and the surrounding cells. Accordingly, we were able to detect the cell-to-cell interactions more efficiently following the initial immune response.

2. Experimental section

2.1. Materials and instrumentations

The chemical reagents were purchased from Sigma Aldrich (US), TCI (Japan), Alfa Aesar (US), Acros Organics (US), Nanocs (US), and Carbosynth (UK). Commercially available reagents and anhydrous solvents were used without further purification. Chemical reactions and purification were performed in an open-air environment at room temperature (25 °C). DBCO-Functionalized Dextran (M.W = 70 kDa) was purchased from Nanocs (Product No. DX70-DB-1, US). 3-Azido-7-hydroxycoumarin was purchased from Carbosynth (Product No. FA31762, UK). Alexa Fluor™ 350-WGA (known as Alexa 350 WGA, *N*-acetyl-D-glucosamine and sialic acid staining reagent) was purchased from Invitrogen (Product No. 1870355B, US). Phycoerythrin (PE)-anti mouse Ly6G Ab (granulocyte marker staining reagent, Biolegend, Product No. B235377, US) was used for staining neutrophils *in vivo*. CellMask™ red (plasma membrane staining reagent, Invitrogen, Product No. H32712, US) were used for the cellular imaging experiment with **HCD-70K**. The pH range was between 4 and 9, including biological pH (7.4) for the pH screening. The pH buffers were purchased from Daejung chem (Rep. of Korea). Human serum (from human male AB plasma, US origin) were purchased from Sigma-Aldrich (Product No. H4522, US).

2.2. Synthesis

*Synthesis of **HCD-70K**.* **HCD-70K** was prepared by metal-free bioorthogonal click-chemistry. DBCO-functionalized dextran (70 kDa) (2.5 mg) and 3-azido-7-hydroxycoumarin (AHC, 40 μg, 0.196 μM) were added in 200 μL methanol at room temperature (25 °C), and vortexed at 37 °C for 72 h. The hydroxy-coumarin-dextran (70 kDa, **HCD-70K**) was then washed 3 times using a centrifuge (15,000 rpm, 3 min) (Centrifuge 5418, Eppendorf, Germany) from methanol to remove un-reacted reagent. The centrifuge e-tube (1.5 mL) was purchased from Axygen (Product No. MCT-150-C, US).

2.3. Characterization of **HCD-70K**

HCD-70K was characterized by using dynamic light scattering (DLS)

analysis, proton nuclear magnetic resonance (^{1}H NMR), and fluorophotometer. Hydrodynamic sizes were measured with a size/zeta-potential analyzer (Malvern Instruments Ltd., Worcestershire, UK). ^{1}H NMR spectra were measured with a Bruker AVANCE III 400 MHz (US). In the NMR spectra, the chemical shifts (δ) are reported in ppm, multiplicities are indicated by s (singlet), d (doublet), t (triplet), dd (double of doublets), and m (multiplet). NMR spectra are referenced to residual dimethyl sulfoxide (DMSO, 2.50 ppm) and H_2O (3.33 ppm).

2.4. Spectroscopic methods

UV–vis absorption spectra were obtained using spectro-photometer (Agilent Technologies Cary 8454, US). Fluorescence spectra were recorded on a spectro-fluorophotometer (SHIMADZU CORP. RF-6000, Japan) with a 1 cm standard quartz cell (internal volume of 1 mL, Hellma Analytics, Germany). All absorption and fluorescence emission spectra were recorded at room temperature (25 °C). Photo-stability of **HCD-70K** was analyzed under constant UV light (365 nm, 3 W, Model RM104, Rayman, Rep. of Korea) in deionized water (DI H_2O) for 60 min at 25 °C. The wavelength spectra were measured by excitation at the maximum absorption wavelength. The time-resolved fluorescence (TRF) signal of the sample solution was measured following 375 nm excitation using a time-correlated single photon counting (TCSPC) method (PicoQuant, Germany). The instrumental response function (IRF) of our TCSPC setup was about 0.1 ns.

2.5. Quantum chemical calculation

All calculations were carried out using the density functional theory (DFT) and time-dependent DFT (TD-DFT) methods at the APFD level with the 6–31 + G(d,p) basis, as implemented in the Gaussian16 package. We calculated the optimized structures, electronic energy levels, frontier orbitals (HOMO and LUMO), electronic absorption spectra of triazole-hydroxy-coumarin (protonated, **THC**) and triazole-hydroxy-coumarin anion (deprotonated, **THCA**). The vibration frequencies of molecules were calculated to check that the optimized structures do not have any imaginary frequencies. The molecular structures of electronic excited **THC** and **THCA** were optimized by the TD-DFT method, and the corresponding electronic emission spectra were calculated. For solvation, we used the integral equation formalism polarizable continuum (IEF-PCM) model.

2.6. Cell study

HeLa cell line (immortalized human cervical cancer) was obtained from the Korean Cell Line Bank. Cells were cultured in Dulbecco's modified Eagle's media (Hyclone, US) supplemented with 10% fetal bovine serum (Hyclone) and 1% penicillin–streptomycin (Gibco). Cultures were incubated at 37 °C in humidified air containing 5% CO_2. For the cell viability assay, approximately 1×10^5 cells were seeded on a 96-well clear bottom plate (SPL Life Science, Rep. of Korea) and incubated for 24 h. After incubation, the cells were treated with **HCD-70K** (0.5–2.5 mg/mL, 0.5 mg/mL interval) for 24 h. The cell viability was then analyzed by using Vybrant® MTT Cell Proliferation Assay Kit (Thermo Fisher, Product No. V13154, US) as per manufacturer's instructions. The absorption level was analyzed at 550 nm by the microplate reader (Multiskan™ FC Microplate Photometer, Thermo Scientific, US). The culture medium was used as a control system. For the confocal laser scanning microscope (CLSM) cellular imaging, approximately 2×10^5 cells were seeded on 35-mm glass bottom confocal dishes (SPL Life Science, Rep. of Korea) and incubated for 24 h. At 80% confluency, the cell was treated with **HCD-70K** (2.5 mg/mL) for 1 h and 6 h respectively, at 37 °C in 5% CO_2. Fluorescence images were visualized by a CLSM (Leica microscope TCS SP5, Germany). Excitation and emission channel; blue (369 nm, 431–490 nm band filter), green (392 nm, 503–562 nm band filter), and red (488 nm, 580–650 nm band filter). CellMask™ red (0.1 μg/mL) was used for the cellular imaging experiment with **HCD-70K**. The ZEN software has been used for the CLSM imaging process (Carl Zeiss, Germany).

2.7. Animal study with TPM in vivo imaging

C57BL/6 mice (2-month old) were purchased from the Orient Bio (Rep. of Korea). LysM-eGFP mice were used to observe neutrophils and some monocytes in various organs [24]. CX_3CR1-GFP mice were used to visualize microglia in the brain [25]. All procedures were conducted in accordance with the guidelines of the Institutional Animal Care and Use Committee (IACUC) of Yonsei University College of Medicine, Rep. of Korea. To clearly visualize and compare the blood vessels injected with **HCD-70K**, cremaster muscle, calvarial bone marrow, cranial window (brain), and dorsal skin chamber window surgery were performed. Each surgical step for different organs was described in the previous studies and some modifications were made to optimize for two-photon *in vivo* imaging [26–29]. All operations were conducted after anesthesia with a dose of zoletil 50 mg/kg (Virbac, France) and rompun 30 mg/kg (Bayer, Germany). Each mouse was kept at 37 °C using a heating plate. Males were used in all imaging of these studies. Prior to imaging, all surgically treated mice were fully anesthetized with the anesthetic conditions used in the surgery described above. The mice were placed in the imaging chamber equipped with a heating plate. **HCD-70K** (2.5 mg/mL) 25 mg/kg dosage was retro-orbitally injected into the mice just before imaging. For blood vessel glycocalyx staining, mice were retro-orbitally injected with pre-warmed (37 °C) Alexa Fluor 350-WGA (100 μg per mouse). In order to stain intravascular neutrophils of CX_3CR1-GFP mice, PE-Anti mouse Ly6G Ab (2 μg) was mixed with **HCD-70K** and then injected in the same manner as described above. Simultaneous multicolor *in vivo* imaging was obtained by laser scanning microscopy (LSM) 7 MP (Carl Zeiss, Germany). Emission filter information; DAPI/SHG, 420–480 nm; GFP/Alexa488, 500–550 nm; and RFP/Alexa 555, 575–610 nm.

Prior to conducting the imaging, Zen 2010 (Black edition, Carl Zeiss, Germany) was used for setting the laser with optimal power and the wavelength was tuned between 780 nm and 840 nm depending on its purpose. With W Plan-Apochromat 20 × /1.0 water immersion lens, 3D images (512 × 512 pixels) were taken at a depth of 40–50 μm with 1 μm slice and for a total of 30 min to 1 h at 60 *sec* intervals. Two-photon *in vivo* imaging data was acquired and analyzed by velocity version 6.3.1 (PerkinElmer, US). The fluorescence intensities of the blood vessels were used as mean values of the region of interest (ROI). The arbitrary unit (a.u) was defined as the fold value divided by the intensity when the **HCD-70K** was not injected. Intensity of the **HCD-70K** at each point was measured by capturing five or more random spots in the blood vessel. All statistical processing was performed with Graphpad prism v7.0 (Graphpad software, US). Results of the analyzed imaging data were presented as standard error of mean (SEM). Two-tailed student's *t*-test was used for comparison between the two groups, and Mann-Whitney *U* test was used when the normal distribution curve was not followed. Statistical significance was defined as p value < 0.05.

2.8. Blood vessel leakage analysis

To quantify the amount of blood leaking from the blood vessel, phosphate-buffered saline (PBS, 200 μL per mice) and **HCD-70K** (2.5 mg/mL) with a dose of 25 mg/kg was retro-orbitally injected into the mice under anesthesia. After 30 min, approximately 1 cm of subcutaneous abdomen was cut and 1 mL of PBS was injected into abdominal cavity. When the PBS was well disbursed, the fluid in the abdominal cavity was extracted with a needleless syringe and put into a tube. In order to measure the absorption and fluorescence intensity, the centrifuge was then operated at 1500 rpm for 3 min to allow the floating cells to settle and to transfer the supernatant.

3. Result and discussion

3.1. Material Design, Synthesis, and characterization

We have designed a new dextran formulation, named **HCD-70K**, that has dextran backbone (M.W = 70 kDa) conjugated with a compact and bright blue-emitting dye; 7-hydroxycoumarin(Fig. 1b). The combination of these components makes it possible to visualize the blood vessels with these features: (i) bright blue-fluorescence (λ_{ex}/λ_{em} = 410/464 nm), (ii) selective staining of blood vessel without leakage, (iii) two-photon excitable for TPM imaging, (iv) deep *in vivo* imaging with 3D image construction, and (v) high biocompatibility.

HCD-70K was prepared by the metal-free bioorthogonal chemistry between dibenzocyclooctyne (DBCO) and 3-azido-7-hydroxycoumarin dye (AHC, Fig. 1b, Fig. S2 in SI) [30–32]. The DBCO moiety allows molecules containing azido groups (–N_3) to be conjugated in the physiological temperature and pH ranges through generating triazole ring. Generally, the DBCO moiety gave poor reactivity to amines or hydroxyls, which are naturally present in many biomolecules, so the non-reacted DBCO residues did not have any issues in bio-applications.

The synthesized **HCD-70K** was firstly characterized by dynamic light scattering (DLS) analysis (Fig. 2a), in order to check the size changes after the conjugation reaction. The average size of **HCD-70K** was 3.49 nm, with no significant size changes in comparison to DBCO-functionalized dextran-70K (3.81 nm). In the ^{1}H NMR analysis, the aromatic protons of DBCO moiety in dextran were monitored at 7.330 ppm, and the peaks became doublet (7.338, 7.325 ppm) after the AHC conjugation. This was most likely due to the AHC conjugation and electron-density changes of DBCO (Fig. S3 in SI). In addition, the CH_2 proton in DBCO moiety at 5.295 ppm became negligible after AHC conjugation, probably due to the conformational change of DBCO. The other major peaks at 1–5 ppm was assigned as protons in the dextran moiety (–CH-, –CH_2). We tried to observe the AHC conjugation to DBCO by mass spectrometry, but the data was inconsistent. So, we verified its conjugation via spectroscopic analysis (see next chapter).

3.2. Spectroscopic study

The absorption and fluorescence spectra of **HCD-70K** were studied in DI H_2O, and its properties were compared to AHC (Fig. 2b, Fig. 2c). Generally, azido-coumarin derivatives are non-fluorescent, because the lone pair of electrons from the azido moiety quenches the fluorescence of coumarin via photo-induced electron transfer (PET) process [33,34]. The fluorescence of coumarin was activated when the triazole ring formed via azido-alkyne or azido-DBCO coupling, so we could monitor the bright blue fluorescence from deprotonated **HCD-70K**, with a peak height of 464 nm (Fig. 2c). We observed within the UV–visible spectra, two major peaks at 348 nm and 400 nm were observed for **HCD-70K**, which correlated with the protonated coumarin and deprotonated coumarin form, respectively (Fig. 2b). In contrast, AHC exists in a protonated form peaked at 342 nm dominantly. DBCO-functionalized dextran-70K itself showed no fluorescence in the given condition (Fig. S4).

We then demonstrated the chemical stability of **HCD-70K** in human serum and the photophysical stability under UV laser (365 nm) irradiation. Significant fluorescence intensity changes of **HCD-70K** in human serum were not observed after 60 min incubation at 37 °C (Fig. S5). This is one of the most important advantages for the blood vessel imaging (Fig. 2d). Surprisingly, **HCD-70K** maintained their fluorescence intensity (> 70%) under strong UV light irradiation (365 nm laser, 3 W at the focal point) in DI H_2O, for up to 60 min incubation (Fig. 2e). In the screening of **HCD-70K** with biologically abundant metal ions (Ca^{2+}, Mg^{2+}, Na^+, K^+, Zn^{+}, Fe^{3+}) and amino acid, only the iron ion showed substantial fluorescence quenching of **HCD-70K**, probably due to the heavy metal effect (Fig. S6 in SI) [35]. The fluorescence intensity of **HCD-70K** was high in the physiological pH ranges (pH 7, 7.4) and basic pHs (pH 9, 11) due to the deprotonation of coumarin moiety; enhanced electron-donating ability (Fig. 2f, Fig. S7 in SI). As expected, the acidic pHs (pH 4, 6) gives a low fluorescence intensity of **HCD-70K** because coumarin exists in a protonated form.

For further investigation, time-resolved fluorescence experiments with **HCD-70K** were carried out. Our TRF experimental results indicate

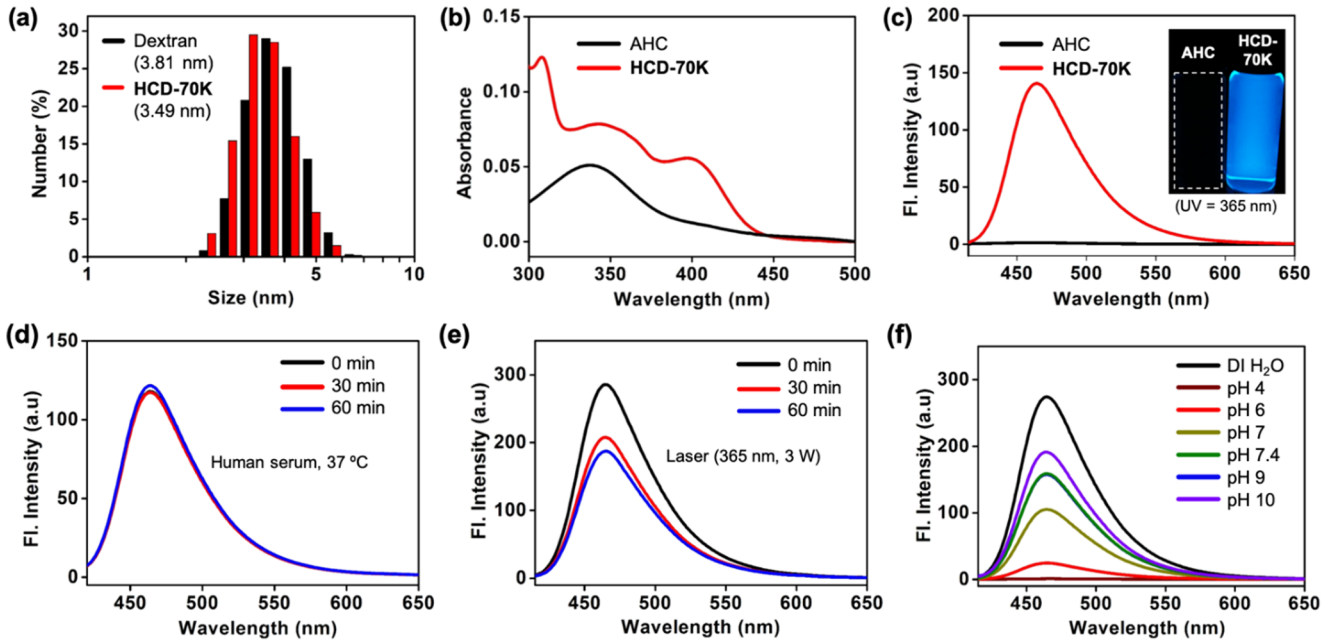

Fig. 2. (a) Mean hydrodynamic diameter (intensity distribution) of DBCO-functionalized dextran (black) and **HCD-70K** (red), measured by dynamic light scattering (DLS). (b, c) UV–vis absorption and fluorescence spectra of AHC (10 μM) and **HCD-70K** (1 mg/mL) in deionized water (DI H_2O) at 25 °C. The inset photo is the fluorescence of AHC and **HCD-70K** in DI H_2O under 365 nm irradiation. (d–f) Fluorescence spectra of **HCD-70K** (250 μg/mL) in (d) human serum at 37 °C for 0–60 min, (e) DI H_2O under the continues 365 nm laser exposure (3 W) for 0–60 min, and (f) various pHs (pH 4, 6, 7, 7.4, 9, 10). The fluorescence spectra were measured at the wavelength of maximum absorbance.

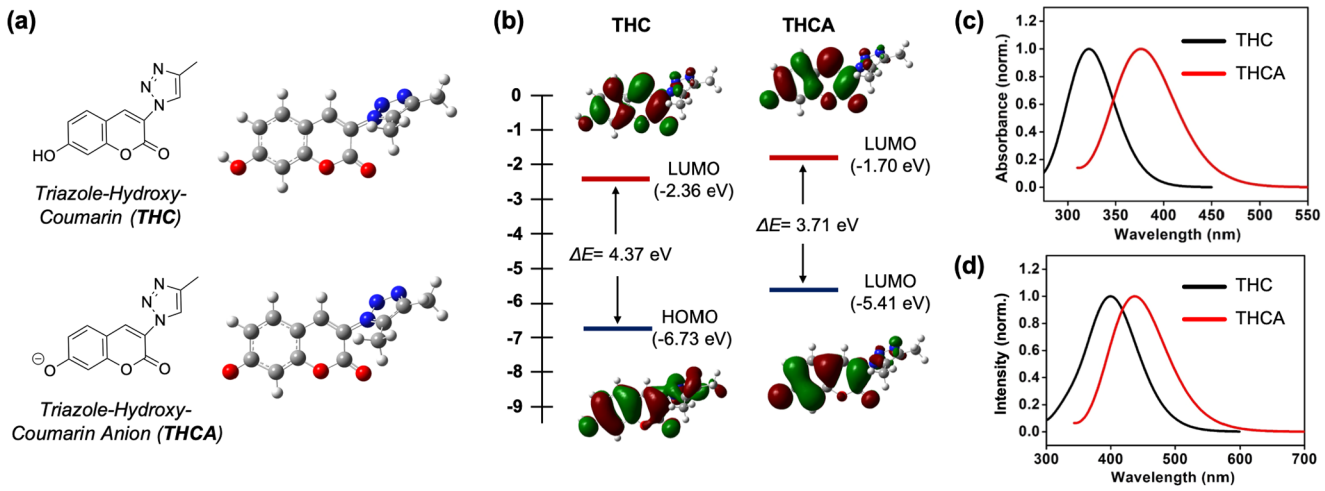

Fig. 3. Results of DFT calculations with APFD/6–31 + G(d,p). (a) Optimized molecular structures of model compound of **HCD-70K**; triazole-hydroxy-coumarin (**THC**, protonated) and triazole-hydroxy-coumarin anion (**THCA**, deprotonated). (b) The HOMO and LUMO orbitals and energies of **THC** and **THCA**. (c, d) Calculated electronic absorption and emission spectra of **THC** and **THCA**.

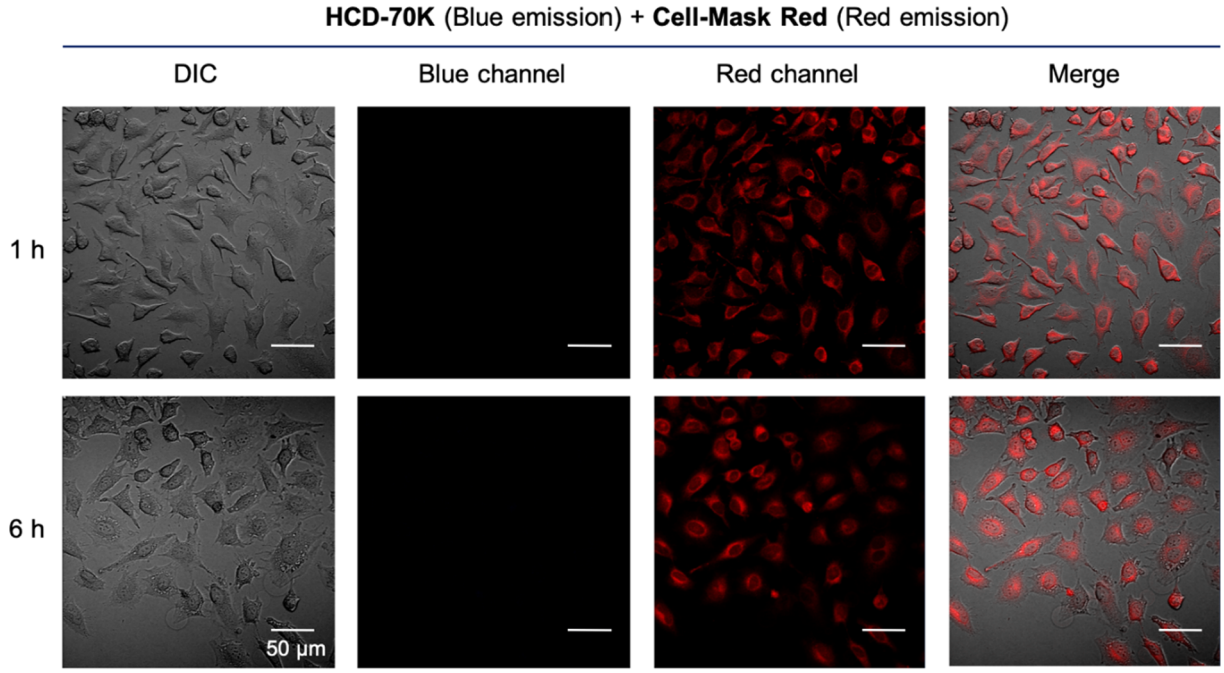

Fig. 4. CLSM images of HeLa cells co-incubated with **HCD-70K** (2.5 μg/mL) and cell membrane imaging agent (Cell-Mask Red, 0.1 μg/mL) for 1–6 h at 37 °C. Excitation wavelength and emission channel; blue (353 nm, 400–550 nm), red (558 nm, 560–700 nm).

that **HCD-70K** undergoes excited-state proton transfer (ESPT) [36] (Fig. S8 in SI). **HCD-70K** in DI H_2O was excited by a 375 nm pulse and its TRF signals were measured as a function of the emission wavelength. The measured TRF signal was analysed by the global standard method to extract the rate constants in the ESPT reaction. The fluorescence lifetimes of **HCD-70K** and its deprotonated form were found to be $\tau = 0.32$ ns and $\tau = 1.9$ ns, respectively, and the ESPT time constant was 0.18 ns. As shown in Fig. S8, the fluorescence of **HCD-70K** from the protonated form was negligibly weak but a strong blue fluorescence results from the deprotonated form of **HCD-70K**.

3.3. Quantum chemical calculation

To understand the optical properties of **HCD-70K**, we used triazole hydroxy-coumarin (**THC**) as a model compound (Fig. 3). **THC** is readily modelled as a fluorophore of **HCD-70K**, and it is deprotonated to produce triazole-hydroxy-coumarin anion (**THCA**). The optimized structures, electronic energies, and HOMO and LUMO orbitals of **THC** and **THCA** in water were calculated by using the DFT method. Electronic absorption and emission spectra were calculated by using the TD-DFT method. First, the HOMO and LUMO orbitals indicate that the intramolecular charged transfer (ICT) character is insignificant when **THC** and **THCA** are electronically excited. Therefore, their optical properties are not substantially dependent on the solvent polarity. Second, the calculated absorption spectra of **THC** and **THCA** matched well with the UV–visible absorption spectra of **HCD-70K** and its deprotonated form presented in Fig. 2b. This result indicates that the absorption and fluorescence spectra should be red-shifted when **HCD-70K** is deprotonated. Finally, the calculated emission spectrum of **THCA** is in good agreement with the fluorescence spectrum of deprotonated **HCD-70K,** while the calculated emission spectrum of **THC** is not observed experimentally. Most importantly the DFT calculation

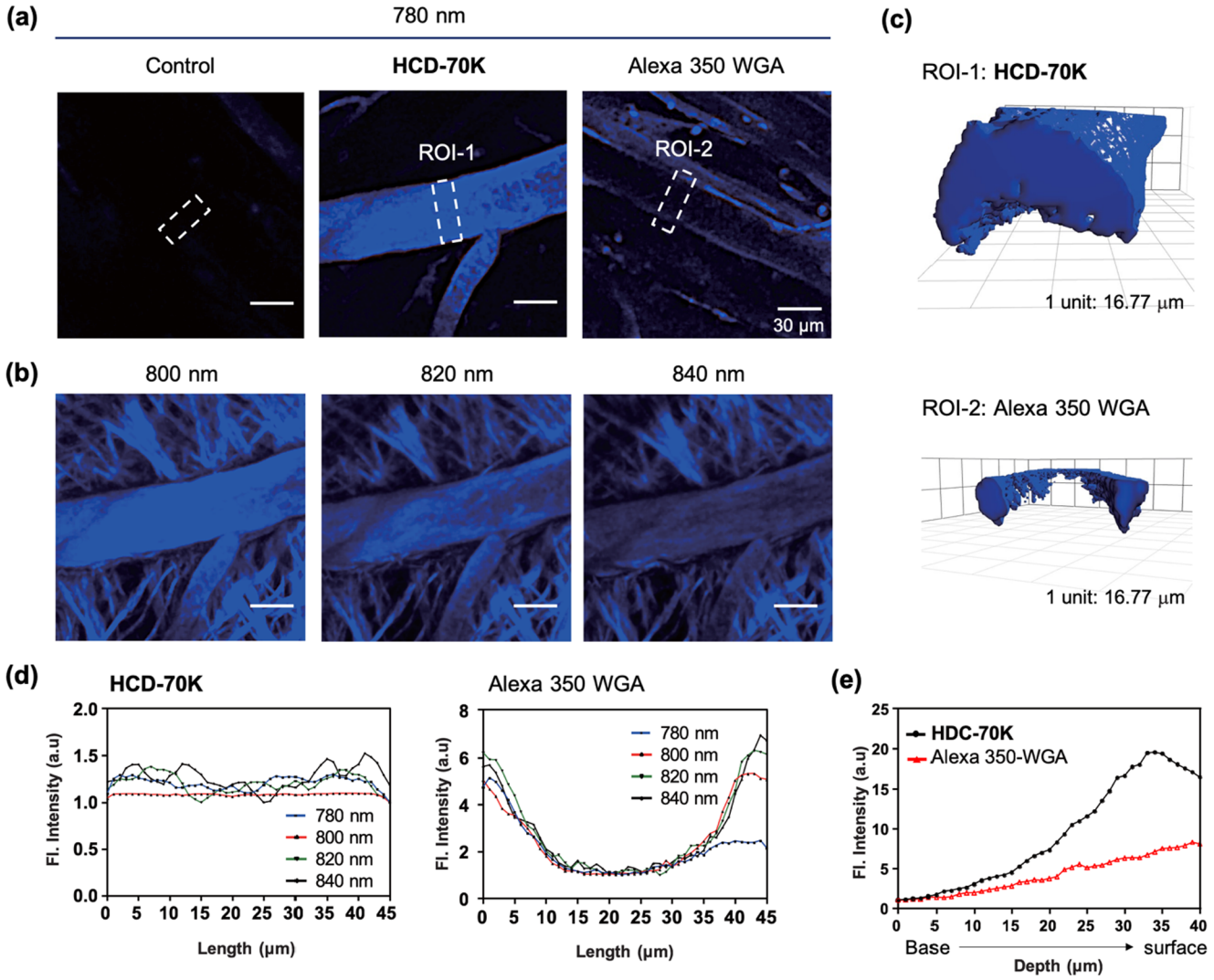

Fig. 5. (a) TPM *in vivo* blood vessel images of two-month old male C57BL/6 mice (2-month-old) were performed after retro-orbital injection of PBS (control, 200 μL/mice), **HCD-70K** (2.5 mg/mL with dose of 25 mg/kg) and Alexa 350 WGA (100 μg/mice), respectively. After 30 min circulation of the injected labeling reagents as described above, the images were recorded at 780 nm two-photon excitation (approximately 50 mW laser at focal plane) with emission channel as described above. The snapshot images obtained from the TPM images show the imaging depth was approximately 50 μm from the surface. (b) Two-photon wavelength-dependent blood vessel imaging with **HCD-70K**. Except the two-photon excitation wavelength, the other experiment condition was the same as panel (a). (c) 3D-constructed images of ROI-1 and ROI-2 in panel (a). (d) Fluorescence intensity plot along with the ROIs in the panel (a) with different two-photon excitation wavelengths. (e) Fluorescence intensity plots along with the depth at ROIs in the panel (a).

confirms that deprotonated **HCD-70K** is responsible for the blue fluorescence.

3.4. Cell permeability study

We evaluated the cell permeability of **HCD-70K** by fluorescence imaging with a confocal laser scanning microscopy (CLSM), because it has a close relation with blood vessel leakage. To clearly observe the cell morphology and track the blue fluorescence signal of **HCD-70K**, HeLa cell (immortalized human cervical cancer) was co-incubated with **HCD-70K** and a commercial dye, Cell-Mask Red that selectively stains the cell membrane red. As shown in Fig. 4, there was no signal in the blue channel, while bright fluorescence was monitored in the red channel, even under a longer incubation time (1–6 h). This result depicts the poor cell permeability of **HCD-70K,** and is considered as an advantage for blood vessel imaging; less leakage of **HCD-70K** through endothelial cells uptake. A low level of cell cytotoxicity (> 80% viability, 0.5–2.5 mg/mL concentration of **HCD-70K**, HeLa cell line) was measured by MTT assay, which was probably due to the low cell permeability of **HCD-70K** (Fig. S9 in SI).

3.5. TPM imaging of blood vessel

We investigated how **HCD-70K** is visible and stable during TPM *in vivo* imaging. Following intravenous injection using the appropriate volumes of **HCD-70K** in a mouse weight dependent manner, TPM *in vivo* imaging was performed in the cremaster muscle, in order to investigate the visibility of **HCD-70K**. **HCD-70K** was more efficiently visible in comparison to Alexa Fluor 350-conjugated wheat germ agglutinin (Alexa 350 WGA), a lectin that binds to *N*-acetyl-D-glucosamine and sialic acid [37]. Alexa 350 WGA was mostly bound to the vessel wall, whereas **HCD-70K** flowed throughout the blood stream, rendering the whole structure of the blood vessel easily visible (Fig. 5a–c). However, both Alexa Fluor 350 and coumarin dyes were excited at short wavelengths and could be overlapped with auto fluorescence of the surrounding tissues, as seen by second harmonic generation (SHG) [38]; regarding this issue, we found that the visibility of the dyes were least hindered by SHG at 780 nm (Fig. 5a, b, Fig. S10).

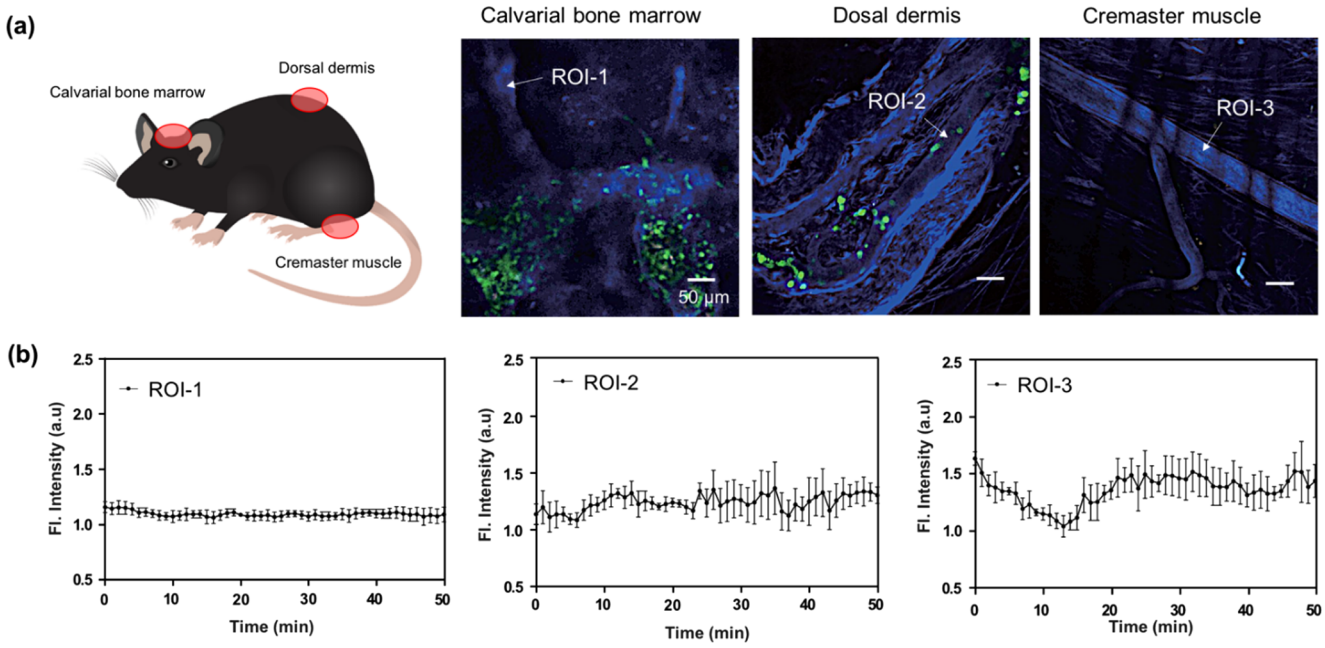

Fig. 6. (a) TPM *in vivo* imaging of blood vessels of two-month old LsyM-GFP mice was performed in calvarial bone marrow, dorsal dermis, and cremaster muscle, for 30 min after retro-orbital injection of **HCD-70K** (2.5 mg/mL with dose of 25 mg/kg). TPM Imaging was performed at 780 nm two-photon excitation (approximately 50 mW laser power at focal plane) with emission channels (as mentioned above). Imaging depth was approximately 40–50 μm for each site, from the surface, respectively. Neutrophil was tagged in green (GFP) and it was imaged at 800 nm, while in the case of calvarial bone marrow imaging, it was taken at 780 nm of TP excitation to avoid bone auto fluorescence. (b) Fluorescence intensity was plotted at each ROI's in the panel (a) for 50 min.

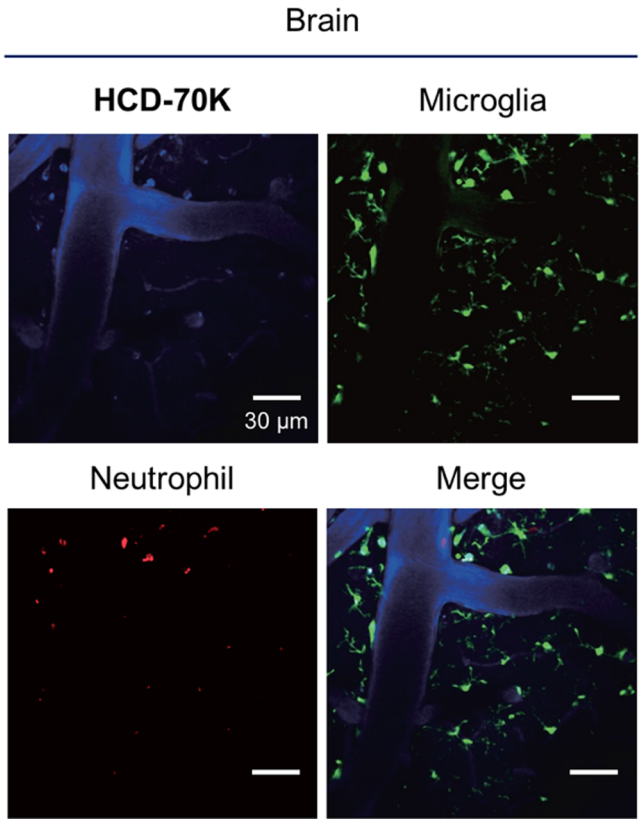

Fig. 7. TPM *in vivo* multi-color imaging of blood vessel, microglias, and neutrophils in brain of two-month old CX_3Cr1-GFP mice after retro-orbital injection of **HCD-70K** (2.5 mg/mL with dose of 25 mg/kg). The images of all channels were recorded simultaneously at 800 nm (50 mW laser power at focal plane) with emission channel (as presented above). Imaging depth was approximately 50 μm from the surface. Microglia was tagged in green (GFP) and neutrophils was stained in red (PE-Ly6G Ab), respectively.

To quantify the distributive properties of **HCD-70K**, a region of interest (ROI, white-dotted square) was selected and fluorescence intensities were measured at various wavelengths. In the case of **HCD-70K**, fluorescence was well distributed throughout the span of the ROI for every two-photon emission wavelength tested. However, when the blood vessel was stained with Alexa 350 WGA, only the vasculature glycocalyx was properly stained. Furthermore, we observed that the fluorescence of the central portion was relatively weak (Fig. 5d). This phenomenon makes sense, due to the fluorescent of Alexa 350 WGA that can only be visualized from the luminal surface of the blood vessel. Because the deep portion of the blood vessel is not easily penetrated by the laser, we also observed changes in the fluorescence intensities as imaging progressed from deep to surface. As the fluorescence intensities of both **HCD-70K** and Alexa 350 WGA got higher towards the surface, the increase in intensity of **HCD-70K** was significantly larger than Alexa 350 WGA, demonstrating that **HCD-70K** is highly advantageous in terms of visibility and efficiency (Fig. 5e).

In order to test the stability and effectiveness of the detection of **HCD-70K**, in the presence of other fluorescent cell populations in various organs, we observed fluorescence in the dorsal dermis and cremaster muscle at 800 nm as well as in the calvarial bone marrow at 780 nm. Despite the aforementioned advantages of using **HCD-70K** at 780 nm, we selected 800 nm for the first two locations, in order to minimize photo-toxicity to other fluorescent cells as much as possible (Fig. 6a). Imaging of the calvarial bone marrow was carried out at 780 nm, since SHG of bone structures obstructed the blood vessel visibility at 800 nm or higher wavelengths. Imaging results yielded consistent fluorescence intensities in all three locations for longer than 50 min, confirming the stability of **HCD-70K** *in vivo* (Fig. 6b). Also, **HCD-70K** was distinctively visible, even alongside other cell populations.

In summary of our results, we concluded that **HCD-70K** was highly fluorescent and photo-stable as observed in various *in vivo* mouse imaging models. **HCD-70K** may serve as an efficient tool to detect fluorescence in the blood vessel and could be particularly utilized in multi-color TPM imaging. Consequently, we could capture CX_3CR1-

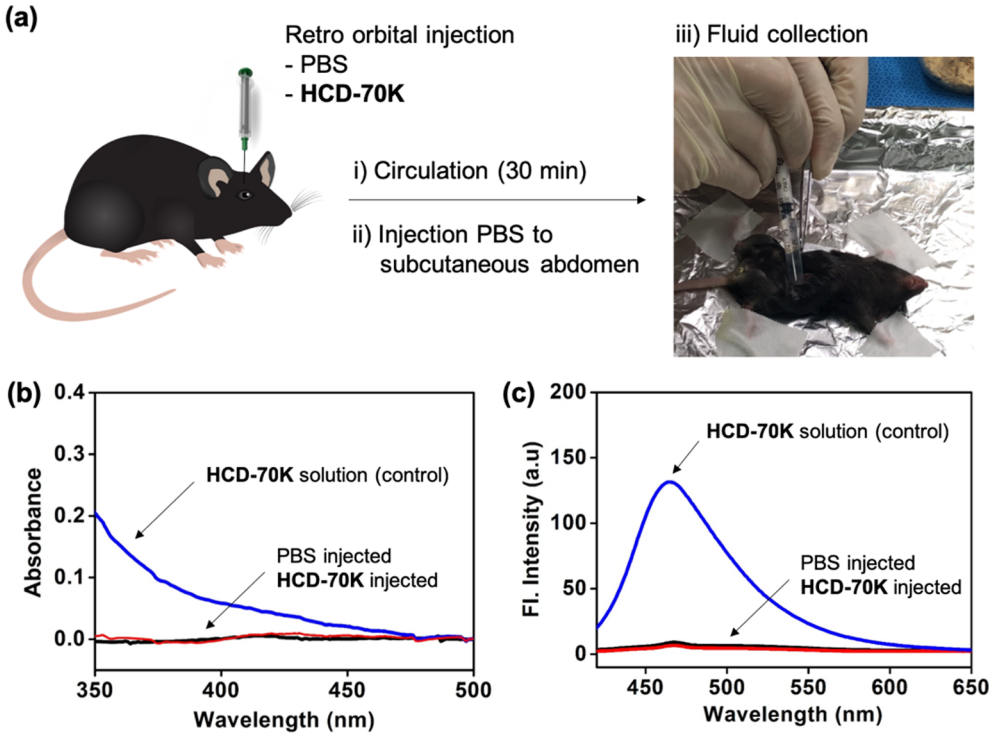

Fig. 8. (a) Experimental scheme for the blood vessel leakage test with **HCD-70K**. PBS (control, 200 μL per mice) and **HCD-70K** (2.5 mg/mL with dose of 25 mg/kg) were injected through retro orbital venous sinus, respectively, to C57BL/6 mice (2-month-old). After 30 min circulation, PBS (1 mL) was injected into subcutaneous abdomen region, and then the fluid was collected (700 μL) using needleless syringe. (b) UV–vis absorption and fluorescence spectra of fluids collected from each mouse. **HCD-70K** solution (in DI H_2O, 0.25 μg/mL) was measured as control (blue). The fluorescence emission spectra were recorded under excitation at 404 nm.

GFP^+ microglia [39], $Ly6G^+$ neutrophils [40] and **HCD-70K** simultaneously in brain imaging at 800 nm emission wavelength (Fig. 7, Fig. S11, Supplementary Movie S1). We confirmed that **HCD-70K** distinctively visualized the blood vessel from cell-to-cell interactions in the blood vessel or extra vascular tissue (Fig. 7).

3.6. Blood vessel leakage test

Stable detection of **HCD-70K** fluorescence *in vivo* was confirmed via *in vivo* TPM microscopy; however, to test whether **HCD-70K** actually remained within the blood vessels, we extracted peritoneal fluid from the peritoneal cavity and measured absorption and fluorescence spectra to detect any potential leakage (Fig. 8a). The supernatant of peritoneal fluid, not including cells, were obtained from mice injected with PBS and those injected with **HCD-70K**. For comparison, the absorption and fluorescence spectra were measured in both supernatants, along with non-injected **HCD-70K**. As a result, both showed no significant absorption and fluorescence signals (Fig. 8b, Fig. 8c) and since non-injected **HCD-70K** had shown absorption and fluorescence as it is, the lack of such indications in peritoneal fluid after **HCD-70K** injection, we confirmed that there was no leakage of **HCD-70K** in the blood vessel. Based on these results, we concluded that **HCD-70K** can be utilized as a stable blood flow labelling tool in the blood vessel without significant risk of leakage, according to the TPM data.

4. Conclusion

In this study, we have developed a bright blue fluorescent dextran, **HCD-70K**, for the tracing of blood vessels with high visibility in two-photon *in vivo* imaging. This blue fluorescent dextran is advantageous for stable vascular visualization especially in combinatorial imaging with red- and green-labeled immune cells and pathogens for two-photon *in vivo* imaging. For the first time, DBCO-functionalized dextran-70K was fabricated with hydroxy-coumarin dye via metal-free bioorthogonal click chemistry, which generated **HCD-70K**. This formulation then circulated through the blood vessel and successfully deciphered the entire structure of the blood vessel. We verified a high stability of **HCD-70K** in human serum and under laser irradiation. The cell uptake assay and blood vessel leakage test proved that **HCD-70K** can only be applied within the blood vessels. The multi-color two-photon *in vivo* imaging ability, with both green-emitting microglia and red-emitting neutrophil presents various research possibilities in the area of vascular diseases.

Acknowledgments

This research was supported by the Bio & Medical Technology Development Program (NRF-2018-M3A9H3021707) and the Brain Research Program (NRF-2016M3C7A1905098) of the National Research Foundation (NRF) of Korea funded by the Ministry of Science & ICT. This research was also supported by Basic Science Research Program through the National Research Foundation (NRF) of Korea funded by the ministry of Education (NRF-2018-R1A6A1A03025124, NRF-2018-R1D1A1B07043383).

Appendix A. Supplementary material

Supplementary data to this article can be found online at https://doi.org/10.1016/j.bioorg.2019.103019.

References

[1] F. Husain-Syed, P.A. McCullough, H.W. Birk, M. Renker, A. Brocca, W. Seeger, et al., Cardio-pulmonary-renal interactions: a multidisciplinary approach, J. Am. Coll. Cardiol. 65 (2015) 2433–2448.
[2] P. Duewell, H. Kono, K.J. Rayner, C.M. Sirois, G. Vladimer, F.G. Bauernfeind, et al., NLRP3 inflammasomes are required for atherogenesis and activated by cholesterol crystals, Nature 464 (2010) 1357–1361.
[3] M. Rabinovitch, C. Guignabert, M. Humbert, M.R. Nicolls, Inflammation and immunity in the pathogenesis of pulmonary arterial hypertension, Circ. Res. 115 (2014) 165–175.
[4] S.H. Kwon, L.O. Lerman, Atherosclerotic renal artery stenosis: current status, Adv. Chronic Kidney Dis. 22 (2015) 224–231.
[5] M. Hjouj, J. Lavee, D. Last, D. Guez, D. Daniels, S. Sharabi, et al., The effect of blood flow on magnetic resonance imaging of non thermal irreversible electroporation, Sci. Rep. 3 (2013) 3088.
[6] Y. Shao, L. Wan, J. Zhang, Z. Li, N. Liu, P. Huang, et al., Post-mortem computed tomography angiography using left ventricle cardiac puncture: A whole-body, angiographic approach, PLoS One 12 (2017) e0183408-e.
[7] W.F. Jiemy, P. Heeringa, J.A.A.M. Kamps, C.J. van der Laken, R.H.J.A. Slart,

E. Brouwer, Positron emission tomography (PET) and single photon emission computed tomography (SPECT) imaging of macrophages in large vessel vasculitis: Current status and future prospects, Autoimmun. Rev. 17 (2018) 715–726.
[8] M. Li, Y. Tang, J. Yao, Photoacoustic tomography of blood oxygenation: A mini review, Photoacoustics 10 (2018) 65–73.
[9] A.Y. Shih, J.D. Driscoll, P.J. Drew, N. Nishimura, C.B. Schaffer, D. Kleinfeld, Two-photon microscopy as a tool to study blood flow and neurovascular coupling in the rodent brain, J. Cereb. Blood Flow Metab. 32 (2012) 1277–1309.
[10] W. Denk, J. Strickler, W. Webb, Two-photon laser scanning fluorescence microscopy, Science 248 (1990) 73–76.
[11] H.M. Kim, B.R. Cho, Small-molecule two-photon probes for bioimaging applications, Chem. Rev. 115 (2015) 5014–5055.
[12] D. Kim, H. Moon, S.H. Baik, S. Singha, Y.W. Jun, T. Wang, et al., Two-photon absorbing dyes with minimal autofluorescence in tissue imaging: application to in vivo imaging of amyloid-β plaques with a negligible background signal, J. Am. Chem. Soc. 137 (2015) 6781–6789.
[13] D. Kim, J. Kang, T. Wang, H.G. Ryu, J.M. Zuidema, J. Joo, et al., Two-photon in vivo imaging with porous silicon nanoparticles, Adv. Mater. 29 (2017) 1703309.
[14] D. Kim, H.G. Ryu, K.H. Ahn, Recent development of two-photon fluorescent probes for bioimaging, Org. Biomol. Chem. 12 (2014) 4550–4566.
[15] S. Ferber, G. Tiram, R. Satchi-Fainaro, Monitoring functionality and morphology of vasculature recruited by factors secreted by fast-growing tumor-generating cells, J. Vis. Exp. (2014) e51525-e.
[16] G. Egawa, S. Nakamizo, Y. Natsuaki, H. Doi, Miyachi Y, Kabashima K. Intravital analysis of vascular permeability in mice using two-photon microscopy, Sci. Rep. 3 (2013).
[17] R.E. Fruge, C. Krout, R. Lu, H. Matsushima, A. Takashima, Real-time visualization of macromolecule uptake by epidermal Langerhans cells in living animals, J. Invest. Dermatol. 132 (2012) 609–614.
[18] S.A. Park, S. Jeong, Y.H. Choe, Y.M. Hyun, Sensing of vascular permeability in inflamed vessel of live animal, J. Anal. Methods Chem. 2018 (2018) 5797152.
[19] J.J. Yao, K. Maslov, S. Hu, L.H.V. Wang, Evans blue dye-enhanced capillary-resolution photoacoustic microscopy in vivo, J. Biomed. Opt. 14 (2009).
[20] A. Abtin, R. Jain, A.J. Mitchell, B. Roediger, A.J. Brzoska, S. Tikoo, et al., Perivascular macrophages mediate neutrophil recruitment during bacterial skin infection, Nat. Immunol. 15 (2014) 45–53.
[21] D. Proebstl, M.B. Voisin, A. Woodfin, J. Whiteford, F. D'Acquisto, G.E. Jones, et al., Pericytes support neutrophil subendothelial cell crawling and breaching of venular walls in vivo, J. Exp. Med. 209 (2012) 1219–1234.
[22] A. Woodfin, M.B. Voisin, M. Beyrau, B. Colom, D. Caille, F.M. Diapouli, et al., The junctional adhesion molecule JAM-C regulates polarized transendothelial migration of neutrophils in vivo, Nat. Immunol. 12 (2011) 761–769.
[23] H. Kataoka, A. Ushiyama, H. Kawakami, Y. Akimoto, S. Matsubara, T. Iijima, Fluorescent imaging of endothelial glycocalyx layer with wheat germ agglutinin using intravital microscopy, Microsc. Res. Techniq. 79 (2016) 31–37.
[24] N. Faust, F. Varas, L.M. Kelly, S. Heck, T. Graf, Insertion of enhanced green fluorescent protein into the lysozyme gene creates mice with green fluorescent granulocytes and macrophages, Blood 96 (2000) 719–726.
[25] S. Jung, J. Aliberti, P. Graemmel, M.J. Sunshine, G.W. Kreutzberg, A. Sher, et al., Analysis of fractalkine receptor CX(3)CR1 function by targeted deletion and green fluorescent protein reporter gene insertion, Mol. Cell Biol. 20 (2000) 4106–4114.
[26] P. Bagher, S.S. Segal, The mouse cremaster muscle preparation for intravital imaging of the microcirculation, J. Vis. Exp. (2011).
[27] M. Alieva, L. Ritsma, R.J. Giedt, R. Weissleder, J. van Rheenen, Imaging windows for long-term intravital imaging: General overview and technical insights, Intravital 3 (2014) e29917.
[28] V.H. Le, S. Lee, S. Lee, T. Wang, W.H. Jang, Y. Yoon, et al., In vivo longitudinal visualization of bone marrow engraftment process in mouse calvaria using two-photon microscopy, Sci. Rep. 7 (2017).
[29] G.M. Palmer, A.N. Fontanella, S.Q. Shan, G. Hanna, G.Q. Zhang, C.L. Fraser, et al., In vivo optical molecular imaging and analysis in mice using dorsal window chamber models applied to hypoxia, vasculature and fluorescent reporters, Nat. Protoc. 6 (2011) 1355–1366.
[30] N.K. Devaraj, The future of bioorthogonal chemistry, ACS Cent. Sci. 4 (2018) 952–959.
[31] D. Zeng, B.M. Zeglis, J.S. Lewis, C.J. Anderson, The growing impact of bioorthogonal click chemistry on the development of radiopharmaceuticals, J. Nucl. Med. 54 (2013) 829–832.
[32] M.R. Karver, R. Weissleder, S.A. Hilderbrand, Bioorthogonal reaction pairs enable simultaneous, selective, multi-target imaging, Angew. Chem. Int. Ed. 51 (2012) 920–922.
[33] Y. Liu, T. Pauloehrl, S.I. Presolski, L. Albertazzi, A.R.A. Palmans, E.W. Meijer, Modular synthetic platform for the construction of functional single-chain polymeric nanoparticles: from aqueous catalysis to photosensitization, J. Am. Chem. Soc. 137 (2015) 13096–13105.
[34] C. Besanceney-Webler, H. Jiang, T. Zheng, L. Feng, D. Soriano del Amo, W. Wang, et al., Increasing the efficacy of bioorthogonal click reactions for bioconjugation: A comparative study, Angew. Chem. Int. Ed. 50 (2011) 8051–8056.
[35] H. Masuhara, H. Shioyama, T. Saito, K. Hamada, S. Yasoshima, N. Mataga, Fluorescence quenching mechanism of aromatic hydrocarbons by closed-shell heavy metal ions in aqueous and organic solutions, J. Phys. Chem. 88 (1984) 5868–5873.
[36] B. Cohen, D. Huppert, Excited state proton-transfer reactions of coumarin 4 in protic solvents, J. Phys. Chem. A 105 (2001) 7157–7164.
[37] V.R. Taqueti, F.A. Jaffer, High-resolution molecular imaging via intravital microscopy: illuminating vascular biology in vivo, Integr. Biol. 5 (2013) 278–290.
[38] X. Jiang, J. Zhong, Y. Liu, H. Yu, S. Zhuo, J. Chen, Two-photon fluorescence and second-harmonic generation imaging of collagen in human tissue based on multiphoton microscopy, Scanning 33 (2011) 53–56.
[39] C. Hierro-Bujalance, B.J. Bacskai, M. Garcia-Alloza, In vivo imaging of microglia with multiphoton microscopy, Front Aging Neurosci. 10 (2018) 218.
[40] J. Neumann, S. Henneberg, S. von Kenne, N. Nolte, A.J. Müller, B. Schraven, et al., Beware the intruder: Real time observation of infiltrated neutrophils and neutrophil—Microglia interaction during stroke in vivo, PLoS ONE 13 (2018) e0193970.